Food Hydrocolloids 165 (2025) 111192

Contents lists available at ScienceDirect

Food Hydrocolloids

journal homepage: www.elsevier.com/locate/foodhyd

Heat-set gelation of milk- and fermentation-derived β-lactoglobulin variants

Zheng Pan[c,1], Remco Kornet[a,1], Sheelagh Hewitt[b], Alan Welman[b], Jeremy P. Hill[b,c], Marcel Wubbolts[a], Stephen Mitchell[b], Warren C. McNabb[c], Aiqian Ye[c], Alejandra Acevedo-Fani[c], Skelte G. Anema[b,c,d,*]

[a] Vivici BV, Alexander Fleminglaan 1, 2613AX Delft, the Netherlands
[b] Fonterra Research and Development Centre, Private Bag 11029, Dairy Farm Road, Palmerston North, 4442, New Zealand
[c] Riddet Institute, Massey University, Private Bag 11222, Palmerston North 4442, New Zealand
[d] School of Food Technology and Natural Sciences, Massey University, Private Bag 11 222, Palmerston North, New Zealand

ARTICLE INFO

Keywords:
Precision fermentation
β-Lactoglobulin
Genetic variants
Amino acid sequence
Rheology
LAOS

ABSTRACT

Milk-derived β-lactoglobulin (mβ-LG) and fermentation-derived β-lactoglobulin (fβ-LG) may slightly differ in their amino acid sequences. This study aims to investigate the heat-set gelling behaviour of mβ-LG (variants A, B, and C) and fβ-LG A variants. Differential scanning calorimetry indicated similar denaturation temperatures for mβ-LG A and fβ-LG A (~75 °C), with mβ-LG C highest (~81 °C) and mβ-LG B intermediate (~78 °C). All fβ-LG A formed translucent gels with a fine-stranded structure, whereas mβ-LG A, B, and C formed opaque gels with a coarse particulate structure. fβ-LG A exhibited delayed gelation onset and lower gel stiffness compared to mβ-LG A. Among mβ-LG's, mβ-LG A showed the highest gel stiffness, followed by mβ-LG B and then mβ-LG C. Rheological analysis showed that fβ-LG A gels were more elastic and ductile compared to mβ-LG A gels, indicated by smaller tan δ values and delayed increases in energy dissipation ratio at higher strain amplitude; mβ-LG B and mβ-LG C gels were less elastic but more ductile compared to mβ-LG A gels. The more elastic and ductile nature of fβ-LG A gels indicates their potential for applications requiring these specific textural properties. By selecting mβ-LG variants from milk and/or utilizing precision fermentation to engineer additional differences, it is possible to tailor the gelation characteristics of β-LG to meet specific functional requirements.

1. Introduction

The growing world population leads to an increasing demand for sustainable food sources, especially high-quality protein. Precision fermentation has been recognized as a novel technology to produce traditional food ingredients, including proteins (Augustin et al., 2023; Hilgendorf et al., 2024; Nielsen et al., 2023). Dairy products are renowned for their high-quality protein content, with whey proteins being a popular food ingredient because of their complete essential amino acid profile and high bioavailability (Gai et al., 2021; Minj & Anand, 2020; Saadi et al., 2024). The major protein of whey is β-lactoglobulin (β-LG) making up about 50% of the protein content (Farrell et al., 2004; Swaisgood, 2003). The market is witnessing an increase in animal-free dairy products, which incorporate fermentation-derived β-LG that claim to be bioequivalent to those found in cow milk. Bioequivalence coupled with a documented history of safe use are important considerations from a regulatory standpoint, as dairy proteins from precision fermentation are typically classified as novel ingredients. Regulatory requirements vary by region, and authorities in several countries, including Canada, China, Singapore and the United States, have already approved one or more dairy proteins from precision fermentation (Food and Drug Administration, 2015; Turck et al., 2024).

However, the potential of precision fermentation is to create tailored variants of β-LG and recent studies have indicated that β-LG from precision fermentation (fβ-LG) could be produced with different amino acid sequences compared to milk-derived β-LG (mβ-LG). For instance, Hoppenreijs et al. (2024) reported the production and functionality of fβ-LG A variants, noting alterations at the N-terminus due to expression. These alterations included a substitution of the N terminal leucine (LIVTQ …) with a prolonged sequence (AKEKGVSLEKRIVTQ …) as well as its

* Corresponding author. Fonterra Research and Development Centre, Private Bag 11029, Dairy Farm Road, Palmerston North, 4442, New Zealand.
E-mail address: skelte.anema@fonterra.com (S.G. Anema).
[1] Equal first authors.

https://doi.org/10.1016/j.foodhyd.2025.111192
Received 20 November 2024; Received in revised form 28 January 2025; Accepted 8 February 2025
Available online 13 February 2025

truncated form (EKGVSLEKRIVTQ …). Similarly, Keppler et al. (2021) produced a fβ-LG B variant with an extension of a single amino acid at the N-terminus (MLIVTQ …) as well as a fβ-LG B variant with the substitution of the N-terminus leucine and isoleucine (LIVTQ …) with both an alanine and serine (ASVTQ …).

The sequential changes at the N-terminus can lead to variations in molecular particle radius, zeta potential, and structural stability at different environmental stresses although the overall structure remained highly similar between mβ-LG and fβ-LG (Keppler et al., 2021). For example, Keppler et al. (2021) reported that the denaturation temperature and zeta potential at pH 7 for fβ-LG B (80.5 °C and −21 mV for fβ-LG B with elongated N-terminus MLIVTQ …, and ~78.2 °C and −21 mV for fβ-LG B with N-terminus substituted amino acids ASVTQ …) was higher than that for mβ-LG B (77.3 °C and −18.6 mV). Those variations could impact the behaviour of proteins in applications, particularly where protein−protein interactions (such as aggregation and gelation properties) are more pronounced (Hoppenreijs et al., 2024).

In bovine milk, mβ-LG exists in several genetic variants. The mβ-LG A and mβ-LG B are the most common in bovine cattle, found at roughly equal frequency. Less common is mβ-LG C, which is at a low but significant frequency in Jersey cattle. There are numerous other rare mβ-LG variants; however, they are found at low frequency and often in less common cattle breeds (Creamer & Harris, 1997; Farrell et al., 2004). The mβ-LG A variant differs from the mβ-LG B variant by two substitutions, with Asp^{64} and Val^{118} in the A variant being Gly^{64} and Ala^{118} in the B variant. The C variant has an additional change from the B variant where Gln^{59} is substituted by His^{59} (Creamer & Harris, 1997; Farrell et al., 2004).

The variants of mβ-LG exhibit distinct responses to thermal processing (Bikker et al., 2000; Huang et al., 1994; Keppler et al., 2014; Manderson, Creamer, & Hardman, 1999; Manderson, Hardman & Creamer, 1998, 1999b; Qin et al., 1999). It has been shown that even subtle changes in the amino acid sequence of mβ-LG can lead to a significant change in functionality such as aggregation and structure of the denatured proteins (Manderson et al., 1998, 1999a, 1999b), functionality in skim milk acid gel systems (Bikker et al., 2000), acid gelling rate and gelation onset temperature (Huang et al., 1994) as well as ligand binding of the native and denatured protein (Keppler et al., 2014). Consequently, a thorough understanding of the gelation properties of mβ-LG and fβ-LG variants is critical as it can guide the sequence selection processes in precision fermentation in order to achieve specific desirable functional properties.

Although an increasing number of research papers on fβ-LG are reported, research focusing on the heat-induced gelling characteristics of fβ-LG is scarce. The gelling characteristics are an important functional property of β-LG, which can have an impact on the textural qualities, sensory qualities, and rheological properties of dairy and other food products. Understanding the gelling properties of different mβ-LG and fβ-LG variants also allows for developing new products with tailored textures and functionalities.

The present study aims to elucidate the heat-induced gelation behaviour of mβ-LG (variants A, B, and C) and a fβ-LG variant (including a comparison of spray dried versus freeze dried protein). It examines how differences in amino acid sequences influence functionality. Additionally, this manuscript gives an in-depth comparison of the rheological properties of the heat-set gels formed from the different β-LG variants using small and large amplitude oscillatory shear (SAOS and LAOS) rheology testing. Insights gained from this study could help steer fermentation-derived dairy protein design and offer valuable information for the potential applications of fβ-LG variants in the dairy industry.

2. Materials and methods

2.1. β-LG samples

The fβ-LG samples were supplied by Vivici (Delft, The Netherlands), produced via precision fermentation using *Komagataella phaffii* (formerly *Pichia pastoris*). *Komagataella* species are heterotrophs that can use, amongst others, glucose, glycerol and methanol as carbon sources. *K. phaffi* has a growth optimum temperature of 30 °C. The purity of individual protein samples was around 80–90%, defined as the weight percentage of protein relative to the total weight of the powder. The three fβ-LG samples were of the same variant A with slight variations in the N-terminal extension, but had different processing histories, with two being produced at laboratory scale, one of them spray dried (fβ-LG SD) and the other freeze dried (fβ-LG FD), and a third being produced at pilot scale and spray dried (fβ-LG PS). The mβ-LG A, B and C variants were purified from milk as has been described previously (Mailliart & Ribadeau-Dumas, 1988; Manderson et al., 1998). Briefly, raw skim milk samples from cows known to be homozygous for mβ-LG A, B and C variants were obtained and the casein was removed by precipitation at pH 4.6. The resultant acid whey was concentrated by repeated undisturbed freeze-thaw cycling, removing the top water layer from the protein rich lower layer. The mβ-LG was separated from the other proteins using the low pH and salt precipitation method (Mailliart & Ribadeau-Dumas, 1988) followed by size exclusion chromatography (Superdex 75, Pharmacia, Uppsala, Sweden), with phosphate buffer (20 mM sodium phosphate, 30 mM NaCl, pH 6.0) to further purify the protein. The purified mβ-LG was ultrafiltered with water until a low and constant conductivity was achieved. The purity of the proteins was about 90%.

Prior to experimentation, solutions of all β-LG variants were dialyzed together against Milli-Q water until a constant low conductivity was achieved. Extensive dialysis was done to ensure that impurities such as minerals would not be an additional variable influencing functionality. The other impurity in the fermentation-derived samples was mannans, which were confirmed to be below 3.17 wt % pre-dialysis, and unlikely to impact gelation behaviour. After dialysis, the β-LG samples were frozen at −80 °C and then freeze dried using a Virtis Freezemobile 25 EL freeze drier (SP Industries Inc., Warminster PA, USA). The samples were stored at −80 °C until use. A description of the samples is given in Table 1.

2.2. HPLC and mass spectrometry analysis of β-LG samples

The protein composition of the mβ-LG and fβ-LG samples was determined by separating protein species using reverse phase HPLC as described previously (Bendall et al., 2024). For the fβ-LG samples, multiple peaks were obtained due to extension of the natural sequence with additional amino acids. The identity of the separated peaks was determined using mass spectrometry as described previously (Bendall et al., 2024), and the quantity of each species was estimated from the relative peak areas of the different species within each sample. The identity of the mβ-LG samples was also confirmed by mass spectrometry. Details of the species present are given in Table 1.

Table 1
Sample names and descriptions.

Abbreviation	Description	Sequence change
mβ-LG A	Bovine β-LG genetic variant A	Reference protein: Asp^{64}, Val^{118}, Gln^{59}
mβ-LG B	Bovine β-LG genetic variant B	Substitution: Gly^{64}, Ala^{118}
mβ-LG C	Bovine β-LG genetic variant C	Substitution: Gly^{64}, Ala^{118}, His^{59}
fβ-LG PS	Freeze-dried fermentation-derived β-LG genetic variant A produced on a pilot scale	N terminal extension: EAEA (53%), AEA (8%), A (26%), other (13%)
fβ-LG FD	Freeze-dried fermentation-derived β-LG genetic variant A produced on a lab scale	N terminal extension: EAEA (70%), AEA (4.5%), EA (1.5%), other (24%)
fβ-LG SD	Spray-dried fermentation-derived β-LG genetic variant A produced on a lab scale	N terminal extension: EAEA (70%), AEA (4.5%), EA (1.5%), other (24%)

2.3. Sample preparation

Solutions of ~15% (w/w) for each β-LG variant were prepared by adding the appropriate quantity of each protein to Milli-Q water (Millipore Corp., Bedford, MA, USA) and stirring until dissolved. The pH of the solutions was adjusted to 7.00 ± 0.05 by slowly adding 1 M NaOH or 1 M HCl solution. The protein concentration of the individual β-LG samples was determined by UV absorbance at 280 nm using 1 cm quartz glass UV cells and the reported extinction coefficient of 0.96 L g^{-1} cm^{-1} (Swaisgood, 1982). An aliquot of each protein solution was diluted by adding Milli-Q water to make the final weight up to 10 g and to give the concentrations of β-LG of 7.5% and 11% (w/w). Subsequently, 150 μL of 25% (w/w) NaCl solution was added and mixed well to achieve a concentration of 64 mM NaCl in the mixture. The 11% protein solutions were used for differential scanning calorimetry experiments, whereas the 7.5% solutions were used for heat-set gelation experiments using rheological techniques.

2.4. Differential scanning calorimetry

The thermal properties of the individual proteins were measured using a differential scanning calorimeter (DSC, DSC-214 Polyma, Netzsch, Selb, Germany). DSC experiments were conducted using protein concentrations of 11% (w/w), which preliminary experiments showed that this gave the optimal signal-to-noise ratio. A ~20 μL aliquot of the protein solutions was weighed into crucibles, and the crucibles were sealed using a crucible sealing press (Netzsch, Selb, Germany). A sealed empty crucible was used as a reference. The samples were scanned from 25 to 100 °C with the temperature ramped at a rate of 7.5 °C min^{-1}, cooled to 25 °C at a rate of 20 °C min^{-1}, and rescanned over the same temperature range and rate to determine whether the proteins had been fully and irreversibly denatured. All DSC analyses were performed under nitrogen, with a dynamic purge flow of 40 mL min^{-1} and a protective flow of 60 mL min^{-1}. The acquisition and handling of the DSC data were performed using Proteus Software Thermal Analysis ver. 8.0.3 (Netzsch, Selb, Germany). Each protein solution was tested twice except for mβ-LG C variant which was tested three times.

2.5. Small amplitude oscillatory shear (SAOS) rheology

The viscoelastic properties of protein solutions (7.5% w/w) were measured in a sand-blasted CC-17 concentric cylinder and corresponding cup geometry on a Physica MCR 302E rheometer (Anton Paar, Graz, Austria). This protein concentration was chosen after preliminary work had shown that 7.5% (w/w) resulted in sufficiently firm gels for comparative purposes so that minimal material was spent. A 4.7 mL aliquot of each protein solution was loaded in the cup and the cylinder was lowered into place. The top surface of the samples was covered by a layer of silicon oil to prevent water evaporation during heating. The solutions were heated from 20 °C to 90 °C at a rate of 5 °C min^{-1}, held at 90 °C for 30 min, cooled from 90 °C to 20 °C at a rate of 5 °C min^{-1}, and finally held at 20 °C for 30 min. The experimental conditions used oscillatory mode at a frequency of 1.0 Hz and a shear strain of 1.0% throughout the rheological measurement. The shear strain was previously confirmed to fall within the linear viscoelastic regime of the gels. The storage modulus (G′) was measured every 0.5 min during gelation. The gelation point was defined as the first measurement at which the G′ was ≥1 Pa. The gelation rate was determined using an exponential decay model as shown in equation (1):

$$Y = \left(Y_{plateau} - Y_0\right)^{-kx} + Y_{plateau} \tag{1}$$

where k = rate constant (min^{-1}), x = heating time (min), $Y_{plateau}$ = storage modulus at infinite time, Y_0 = first storage modulus point at which the storage modulus was greater than 1 Pa.

After completion of the temperature cycle, the obtained gels were subjected to a frequency sweep from 0.01 to 10 Hz at a strain of 1.0% at 20 °C. The storage modulus (G′), loss modulus (G″) and tan δ dependency on the frequency were recorded. Each protein solution was tested in duplicate. The method is adopted from Kornet et al. (2021) with some modifications.

2.6. Large amplitude oscillatory shear (LAOS) rheology

LAOS rheology tests were conducted after the frequency sweep. Strain sweep tests were carried out from 0.1 to 1000% incrementing in a logarithmic manner at a frequency of 1 Hz and 20 °C. The storage modulus (G′) and shear stress dependence on strain were recorded. In addition, the recorded signals of strain, stress, and shear rate, which oscillated in response to the applied sinusoidal strain, were utilized to generate Lissajous plots. The MITlaos program (Ewoldt et al., 2007) was used to collect the original stress and strain data to analyze the Lissajous curve, the third harmonic viscoelastic moduli, and the Chebyshev coefficient.

The area enclosed in a Lissajous curve can be interpreted as the energy dissipated per unit volume during one complete cycle of the oscillatory strain that is imposed. The energy dissipated per unit volume in a single cycle (Equation (2)) is a function only of the first-order viscous Fourier coefficient (G''_1; calculated from the intensity and phase of the first harmonic):

$$E_d = \int \sigma d\gamma = \pi G''_1 \gamma_0^2 \tag{2}$$

The energy dissipated by a perfect plastic material in a single cycle (Equation (3)) is equal to

$$(E_d)_{pp} = 4\gamma_0 \sigma_{max} \tag{3}$$

for a given strain amplitude (γ_0) and a maximum stress (σ_{max}). The Lissajous curve for a perfect plastic material has a rectangular shape. This shape corresponds to a material that initially gives a perfectly rigid response, at the maximum deformation of the cycle (lower left and upper right corners), and subsequently yields, and displays a constant stress (σ_{max}), independent of the strain in the rest of the cycle (i.e. purely plastic behaviour).

Comparing the actual dissipated energy to the perfect plastic dissipation gives the energy dissipation ratio (ϕ) as proposed by Ewoldt et al. (2010; Equation (4)).

$$\Phi = \frac{E_d}{(E_d)_{pp}} = \frac{\pi G''_1 \gamma_0}{4\sigma_{max}} \tag{4}$$

2.7. Protein charge calculation

Changes in the net charge as a function of pH for the genetic mβ-LG variants of both the native structure (one free thiol and two disulphide bonds) or the reduced protein (five free thiol groups) as well as the fermentation-derived fβ-LG (assuming 100% EAEA N-terminal extension) were calculated using the Protein Calculator (2013) from the Scripps Research Institute.

2.8. Confocal microscopy analysis of gelled samples

The microstructure of the gelled mβ-LG A and fβ-LG FD was analysed using confocal laser scanning microscopy (CLSM) as detailed by Bendall et al. (2024). Briefly, sections of the heat-set gels of mβ-LG A and fβ-LG FD were placed on individual concave microscope slides and proteins were stained with the fluorescent dye Fast Green FCF (0.2% in polyethylene glycol, Sigma-Aldrich, Auckland, New Zealand). Coverslips were placed over the samples, and the microstructure was examined using a ZEISS LSM 800 Airyscan confocal microscope (Carl Zeiss, Oberkochen, Germany). Laser excitation parameters were set at 633 nm for the Fast Green probe. Images were captured from randomly selected areas of each sample.

2.9. Replication and statistical analysis

All experiments reported were replicated for both sample treatments and sample analyses. Standard deviations were used where appropriate to indicate the variability between repeated experiments or measurements. Analysis of variance (ANOVA) using GraphPad Prism Statistical Software 8.4.1 (Boston, MA, US) was conducted for statistical analysis where appropriate.

3. Results and discussion

3.1. Differential scanning calorimetry

The denaturation temperatures and heat enthalpies are shown in Table 2. No renaturation was observed for all β-LG samples in the rescan step (data not shown), indicating all proteins were irreversibly denatured. The denaturation temperatures (T_d) of both the mβ-LG and fβ-LG variants ranged from 75 to 80 °C, which is consistent with the previously reported T_d range for mβ-LG of between 70.4 and 85.5 °C at neutral pH (Paulsson & Dejmek, 1990; Paulsson et al., 1985; Ruegg et al., 1977). For the mβ-LG variants, mβ-LG C showed the highest T_d at 80.7 °C, followed by mβ-LG B (77.8 °C) and mβ-LG A (75.8 °C; Table 2). These results are in agreement with previous reports on the thermal stability of mβ-LG variants, which showed the order mβ-LG A < mβ-LG B < mβ-LG C (Keppler et al., 2014; Panick et al., 1999; Sawyer, 1968).

Small, and in some cases non-significant, differences in T_d were found among mβ-LG A, fβ-LG PS, fβ-LG FD and fβ-LG SD, indicating that the fβ-LG A used in this study has comparable thermal denaturation properties compared to mβ-LG A. However, mβ-LG A and fβ-LG SD showed a significantly lower enthalpy compared with fβ-LG PS and fβ-LG FD. The differential enthalpic requirements for denaturation between mβ-LG A and fβ-LG A could be attributed to variations in structural stability and intramolecular interactions arising from their different amino acid sequences (Manderson et al., 1998). The reduced enthalpy observed for fβ-LG SD, in comparison to fβ-LG PS and fβ-LG FD, could be explained by the partial denaturation of the fβ-LG during the lab-scale spray drying process (Anandharamakrishnan et al., 2007), which would result in a lower proportion of native fβ-LG SD during the DSC analysis.

The comparable T_d between mβ-LG A and fβ-LG A found in this study contrasts with the observations made by Keppler et al. (2021), who showed the T_d at pH 7 of fβ-LG B (~80.5 °C for fβ-LG B with an additional methionine at the N-terminus and ~78.2 °C for fβ-LG B with leucine and isoleucine substituted by alanine and serine, respectively, at the N-terminus) was higher than that for mβ-LG B (77.3 °C). One possible explanation for this discrepancy could lie in the variations of the amino acid sequences at the N-terminus; modifications at this site can either enhance or compromise protein stability, as suggested by Schultz and Baldwin (1992) and Chaudhuri et al. (1999). Furthermore, differences in the purification protocols for fβ-LG (Keppler et al., 2021), as well as different DSC conditions used across studies, such as protein concentration and salt concentrations (Anema et al., 2006), might impact the thermal properties of proteins.

3.2. SAOS rheological properties

β-LG samples (7.5% protein) with NaCl added (64 mM) were tested for heat-set gel formation using a temperature cycle from 20 °C to 90 °C and back to 20 °C (Fig. 1, Table 1). For the mβ-LG A, mβ-LG B and mβ-LG C variants (Fig. 1A), when the temperature was raised to ~90 °C, the increase in G′ indicated that the samples had started to gel, and the G′ slowly increased on continued holding at 90 °C. On cooling to 20 °C, the G′ linearly increased with decreasing temperature, and then remained constant on holding at 20 °C for 30 min. At any time after gelation, the G′ for mβ-LG A was the highest and for mβ-LG C was the lowest, with mβ-LG B intermediate. The final G′ after the complete heat-hold-cool-hold cycle was about 19, 000 Pa for the mβ-LG A, 11, 000 Pa for the mβ-LG B and 5, 000 Pa for mβ-LG C. An examination at the point at which the samples gelled showed that the mβ-LG B started gelling earlier than the mβ-LG A and mβ-LG C at about 17 min (corresponding to a temperature of about 85 °C), whereas both mβ-LG A and mβ-LG C started gelling at 18.5 min (corresponding to a temperature just below 90 °C). The *k* after the point of gelation was similar for the three mβ-LG variants, although mβ-LG A was slightly slower than mβ-LG B with mβ-LG C intermediate (Table 2). The appearance of the gels for the three variants was similar being very opaque and milky white (Fig. 2A–C). The CLSM image of the gel from mβ-LG A (Fig. 2G) exhibited an inhomogeneous, coarse structure of aggregated protein material interspaced with distinct channels indicating a particulate network structure consistent with the opaque milky white appearance of the gel (Fig. 2A).

For each genetic variant, the frequency sweeps of the set gels after the temperature cycle and at 20 °C produced parallel lines for G′ and G″ against frequency on a double log plot. In all cases and at each frequency, the G′ was substantially higher than the G″ (Fig. 3A(i)). As with the gelation curves, the G′/G″ were highest for mβ-LG A and lowest for mβ-LG C, with mβ-LG B intermediate; however, despite the large differences in G′/G″ the slopes of the curves with frequency were very similar indicating that the time-dependent behaviour of the samples to deformation was similar, and therefore they possessed a similar gel network structure. This was supported by a power law fitting of $G'–\omega^n$, (results not shown), which produced only minor differences in *n* indicating similar gel types. An entangled network would show a G″ > G′ at low frequencies and the material can flow as high viscosity fluids. As the frequency increased, there would be a crossover where G′ becomes greater than G″ and the material acts more solid- or gel-like rather than a viscous liquid. In a true gel, the G′ is greater than G″ at all frequencies and are parallel lines that are insensitive to frequency (Hairunnisa Ramli et al., 2022; Picout & Ross-Murphy, 2003). For the gels formed from mβ-LG A, mβ-LG B and mβ-LG C, the G′ being greater than G″ at all frequencies, the low dependence of the G′ and G″ curves on frequency, and the parallel nature of the G′ and G″ curves indicate the samples are close to a true gel structure rather than an entangled network (Fig. 3). These gelation results and the final G′/G″ values are in the opposite order of the denaturation temperatures obtained from DSC, where the T_d for mβ-LG A was lower than mβ-LG C variant with mβ-LG B intermediate (Table 2).

Table 2
Denaturation temperature (T_d), enthalpy, onset time of gelation, rate constant (*k*) of gel formation, and final stiffness (G′) at 90 °C and 20 °C of heat set gels. The R^2 is the fit to the exponential decay model (equation (1)).

Abbreviation	T_d (°C)	Enthalpy (J g^{-1} protein)	Onset of gelation (min)	*k* after gelation onset (min^{-1})	R^2	G′ at 90 °C (Pa)	G′ at 20 °C (Pa)
mβ-LG A	75.8 ± 0.5^b	8.260 ± 0.035^a	18.5	0.099^c	0.9959	4406 ± 128^b	19024 ± 586^c
mβ-LG B	77.8 ± 0.2^c	16.595 ± 0.086^d	17	0.123^d	0.9929	1942 ± 270^a	11565 ± 1644^b
mβ-LG C	80.7 ± 0.2^d	13.170 ± 0.279^c	18.5	0.114^{cd}	0.9893	741 ± 6^a	5029 ± 15^a
fβ-LG PS	75.3 ± 0.2^{ab}	12.477 ± 0.950^{bc}	23	0.044^b	0.9985	942 ± 77^a	4055 ± 189^a
fβ-LG FD	75.1 ± 0.0^a	11.314 ± 0.177^b	23.5	0.034^a	0.9984	711 ± 49^a	3292 ± 42^a
fβ-LG SD	75.5 ± 0.3^{ab}	8.270 ± 0.120^a	23	0.033^a	0.9988	806 ± 148^a	4411 ± 149^a

Means followed by different superscript letters within a column are significantly different at $p < 0.05$.

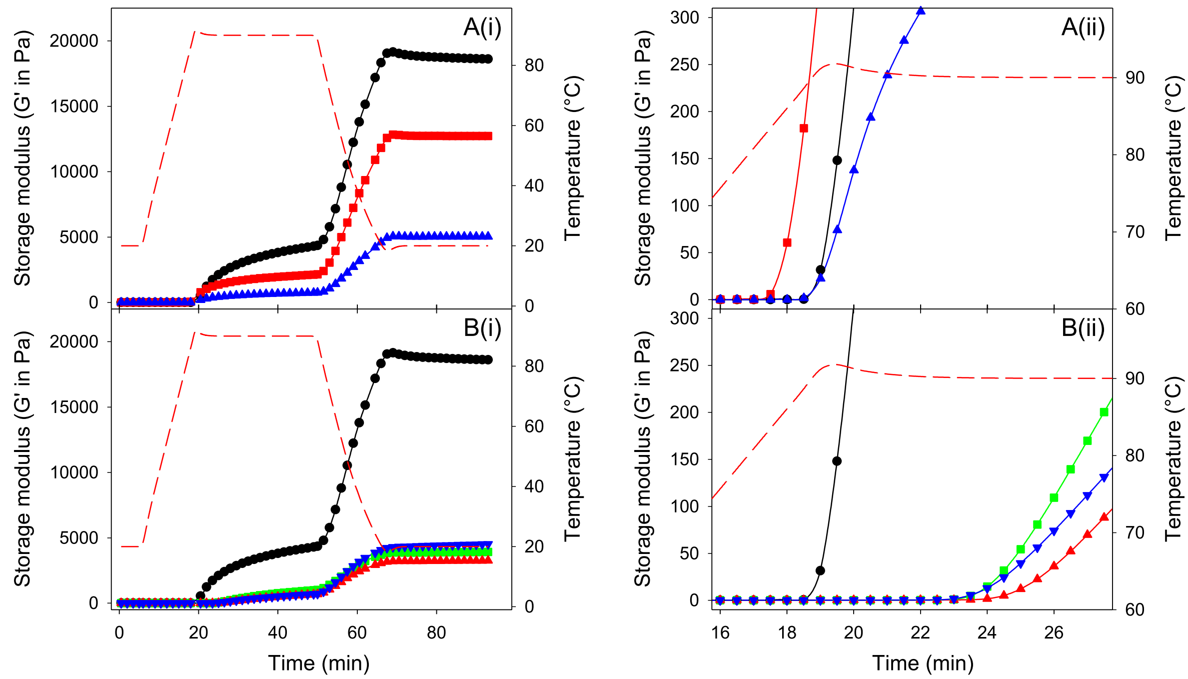

Fig. 1. Changes in the rheological properties of the β-LG samples during heating. The β-LG samples (7.5% w/w in water with 64 mM NaCl) were held at 20 °C for 5 min, heated from 20 °C to 90 °C at a rate of 5 °C min^{-1}, held at 90 °C for 30 min, cooled from 90 °C to 20 °C at a rate of 5 °C min^{-1}, and finally held at 20 °C for 30 min. A(i) and A(ii): mβ-LG A (●), mβ-LG B (■) and mβ-LG C (▲). B(i) and B(ii): mβ-LG A (●), fβ-LG PS (■) fβ-LG FD (▲), fβ-LG SD (▼). A(i) and B(i) show the full temperature/time range whereas A(ii) and B(ii) show a reduced temperature/time range.

The tan δ with frequency (ratio of G″/G′) showed a similar curved behaviour for all three mβ-LG variants with a higher tan δ at low and high frequencies and a lower tan δ at the intermediate frequency (Fig. 3A(ii)). As the tan δ is the ratio of energy lost (viscous component) to energy stored (elastic component) during the oscillations, these results indicate that slightly more oscillation energy is dissipated at low and high frequencies than at intermediate frequencies, which may imply less microstructural rearrangements at the intermediate frequency range. The tan δ curves for mβ-LG B and mβ-LG C were the same whereas that of mβ-LG A was displaced to lower tan δ at each frequency. This suggests that at all frequencies, more oscillation energy is stored (elastic component) and less energy is dissipated (viscous component) for the gels from mβ-LG A variant when compared with those from mβ-LG B and mβ-LG C.

Changes in the net charge as a function of pH for the genetic mβ-LG variants of both the native structure (one free thiol and two disulphide bonds) or the reduced protein (five free thiol groups) were calculated (Fig. 4). Results show a significant difference in the isoelectric pH and a significant charge difference at pH 7.0, where these gelation experiments were conducted (Fig. 4). For the native protein, the isoelectric pH shifted from pH 4.86 to 4.92 to 5.01 and the charge at pH 7 shifted from −8.6 to −7.6 to −7.4 for the mβ-LG A, mβ-LG B and mβ-LG C variants, respectively. The isoelectric pH for each variant was unchanged in the reduced form of mβ-LG when compared with the native structure as expected, as the free thiols do not carry charge at these pH's; however, the charge at pH 7.0 was shifted slightly (by −0.1) in the reduced forms (Fig. 4). These charges are in the same order as the gel stiffness (Table 2), with mβ-LG A having the highest negative charge and highest stiffness, mβ-LG C having the lowest negative charge and lowest stiffness and mβ-LG B having intermediate charge and stiffness.

There is evidence that the mβ-LG variants undergo denaturation and aggregation differently upon heating. Manderson et al. (1998), based on gel electrophoresis techniques, reported that mβ-LG C formed a large number of high molecular weight aggregates when heated, with mβ-LG B forming an intermediate level of aggregates and mβ-LG A the smallest number of large aggregates. Other studies showed a 1:1 relationship between surface hydrophobicity (ANS fluorescence) or thiol availability (DTNB reactivity) and the loss of native protein, but not with the loss of SDS-monomeric protein, and this behaviour was similar for all three mβ-LG variants (Manderson, Hardman, & Creamer, 1999). Tryptophan fluorescence did not show a similar relationship with the loss of native mβ-LG and it was suggested that mβ-LG A may denature and aggregate through a different mechanism to mβ-LG B and mβ-LG C (Manderson, Hardman, & Creamer, 1999). Similarly, the circular dichroism spectra of heated mβ-LG variants were different with mβ-LG C being more stable than mβ-LG B with mβ-LG A intermediate (Manderson, Creamer, & Hardman, 1999). Thresher and Harris (1997) in a study on the interaction of mβ-LG variants with a specially activated DTNB-κ-casein complex showed that mβ-LG A was most reactive with the DTNB-κ-casein, with mβ-LG B intermediate and mβ-LG C least reactive. These suggest that the exposure of a reactive thiol group on heating was in the order of mβ-LG A > mβ-LG B > mβ-LG C.

In addition to the net charge differences between the genetic variants, previous studies have suggested that differences in the denaturation and aggregation of mβ-LG variants could be a consequence of structural differences in the proteins induced by the amino acid substitutions. For example, for mβ-LG A and mβ-LG B, the Val^{118} to Ala^{118} substitution could induce a cavity, and the Asp^{64} to Gly^{64} substitution could cause a changed charge distribution in the CD loop within the mβ-LG structure. The Asp^{64} to Gly^{64} substitution also results in a greater negative charge close to the Cys^{66}-Cys^{160} disulphide bond in the case of mβ-LG A, likely hindering intermolecular thiol-disulphide interchange reactions with thiolate anions (Manderson, Hardman, & Creamer, 1999). With the mβ-LG C having a His^{59} instead of the Gln^{59} in the mβ-LG A/mβ-LG B may produce an additional salt bridge between strand B and C to stabilize the structure (Manderson et al., 1998, 1999a).

For the heat set gelation behaviour of the fβ-LG, three samples were tested from two separate batches. The fβ-LG PS and fβ-LG FD samples were freeze dried from different batches whereas the fβ-LG SD sample was the same batch as the fβ-LG FD sample, but spray dried instead of freeze dried. Although all fβ-LG samples were predominantly with an N-terminus extension of EAEA + natural sequence, there were some

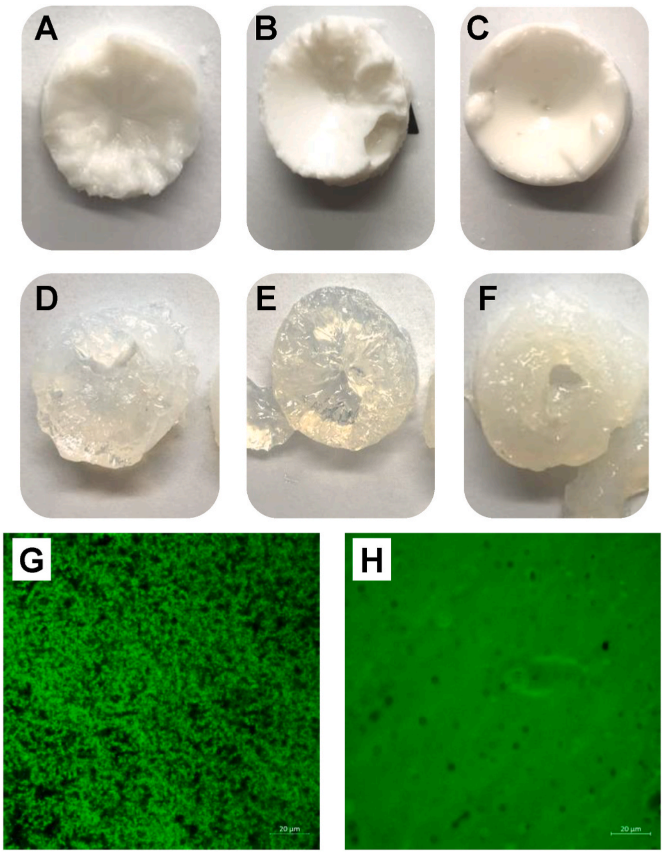

Fig. 2. Appearance (A–F) and microstructure (G and H) of the heat-set gels. The gels were prepared from β-LG solutions (7.5% w/w in water with 64 mM NaCl) that were held at 20 °C for 5 min, heated from 20 °C to 90 °C at a rate of 5 °C min^{-1}, held at 90 °C for 30 min, cooled from 90 °C to 20 °C at a rate of 5 °C min^{-1}, and finally held at 20 °C for 30 min. A: mβ-LG A. B: mβ-LG B. C: mβ-LG C. D: fβ-LG PS. E: fβ-LG FD. F: fβ-LG SD. Confocal images of heat-set gels formed from (G) mβ-LG A and (H) fβ-LG FD.

truncations that removed N-terminal amino acids to give some AEA + natural sequence as well as some further truncations as minor species. These distributions were slightly different between the two batches (Table 1). Overall, the three fβ-LG samples produced similar heat-set gelation curves, and these curves were displaced to lower G′ than those from the mβ-LG A from which this fβ-LG protein was derived (Fig. 1B). The gelation curves were actually similar in behaviour, albeit slightly lower in G′ at any given time, to curves for mβ-LG C (Fig. 1B(i)). Similarly, the final G′, at about 3,300 to 4,400 Pa, was slightly lower than mβ-LG C (about 5,000 Pa), but only about one quarter that of mβ-LG A (at about 19,000 Pa).

When looking at the point at which the samples gelled (Fig. 1B(ii)), the fβ-LG variants gelled much later than the mβ-LG variants, with mβ-LG A gelling at 18.5 min (corresponding to a temperature just below 90 °C), whereas the fβ-LG PS and fβ-LG SD samples gelled at 23 min (about 4 min after reaching 90 °C) and the fβ-LG FD sample gelled at about 23.5 min (after about 4.5 min at 90 °C), implying higher heat stability for the fβ-LG compared with mβ-LG. The *k* after the point of gelation was also markedly lower than the mβ-LG variants at between 0.033 and 0.044 Pa min^{-1}, compared with mβ-LG A at 0.1 Pa min^{-1} (Table 2). An interesting aspect was that the appearance of the heat set gels was markedly different between the mβ-LG and fβ-LG. Unlike the mβ-LG variants that produced opaque and milky white gels, the fβ-LG produced transparent/translucent gels (Fig. 2D–F). The CLSM image of the fβ-LG FD gel displayed a homogeneous gel structure that lacked any discernible individual structural features (Fig. 2H). The visual appearance and the microstructural images suggested that the gels from the fβ-LG were composed of a fine-stranded network with minimal light scattering rather than a particulate or micro-phase separated network (Khalesi et al., 2021; Saikhwan et al., 2010). This observation aligns with the lower stiffness of the fβ-LG gels, as previously reported by Stading and Hermansson (1990) in their comparison of fine-stranded and particulate β-LG gels.

As with the mβ-LG A, mβ-LG B and mβ-LG C, the frequency sweeps of the set gels for the fβ-LG samples had G′ greater than G″ at all frequencies, the G′ and G″ curves were parallel to each other and the G′ and G″ were relatively frequency independent indicating a true gel structure. As with the gels from the mβ-LG variants, a power law fitting of G′–ω^n, (results not shown) produced only minor differences in *n* indicating similar gel types for all β-LG samples. Interestingly, where mβ-LG A, mβ-LG B and mβ-LG C showed a small increase in G′ and G″ with increasing frequency, the translucent and fine-stranded gels from fermentation-derived samples showed less dependence on frequency, especially for G″, indicating they were closer to a true gel than the mβ-LG variants. This is consistent with the findings of Khalesi et al. (2021), who showed that particulate whey protein gels had a stronger G′ – frequency dependency due to a larger viscous component contribution. The fβ-LG PS and fβ-LG SD samples had slightly higher G′ and G″ than the fβ-LG FD sample at all frequencies, and these were markedly lower than the mβ-LG A sample. These curves were closer to, but slightly lower than the mβ-LG C gel at all frequencies, as was observed during the gel formation (Fig. 1).

The tan δ for the three fβ-LG samples showed the same behaviour with frequency; however, this was different when compared with the mβ-LG A, mβ-LG B and mβ-LG C gels (Fig. 3). Where the mβ-LG variants showed a higher tan δ at low and high frequencies and a lower tan δ at intermediate frequencies, the fβ-LG proteins showed a high tan δ at low frequency, with tan δ decreasing with increasing frequency to a minimum at about 1 Hz, with little further change as the frequency increased further. This indicates that slightly more of the oscillation energy is dissipated at the low frequencies than at the intermediate and high frequencies. The tan δ curves for the fβ-LG PS and fβ-LG FD gels were similar, whereas that of the fβ-LG SD gel was displaced to higher tan δ at each frequency. This indicates that at all frequencies more of the oscillation energy is stored (elastic component) and less energy is dissipated (viscous component) for the gels from the fβ-LG PS and fβ-LG FD when compared with the fβ-LG SD gel. The fβ-LG PS and fβ-LG FD gels had a much lower tan δ than the mβ-LG A gel at all frequencies, indicating that the gels from these samples were more elastic and less viscous than those from mβ-LG A. These observations can be likely explained by the higher microstructural homogeneity of a fine-stranded network. The gels from the fβ-LG SD sample had a higher tan δ than the gel from mβ-LG A at frequencies up to about 0.5 Hz and a lower tan δ at higher frequencies, indicating the fβ-LG SD gel had a higher viscous to elastic component than the gel from mβ-LG A at the low frequencies, but a lower viscous to elastic component at higher frequencies.

The addition of EAEA to the N-terminal of β-LG A to make the fermentation-derived protein has a marked effect on the charge of the protein. The isoelectric pH is shifted from pH 4.86 in the mβ-LG A to pH 4.75 in the fβ-LG, whereas the charge at pH 7 is shifted from −8.6 in the mβ-LG A to −10.6 in the fβ-LG (Fig. 4). In contrast to the gelling behaviour, where the gelation point was later for the fβ-LG, DSC showed that the temperature for denaturation, T_d, for the fβ-LG PS, fβ-LG SD and fβ-LG FD were similar to (or slightly lower) when compared with mβ-LG A (Table 2), indicating that the unfolding temperature of the protein was similar between the milk-derived and fermentation-derived samples. The enthalpy for the fβ-LG PS and fβ-LG FD samples was higher than the mβ-LG A, whereas the fβ-LG FD and mβ-LG A were similar.

The observation that the gelling was occurring later for the fermentation-derived protein suggest that the interaction of the unfolded protein to form the gel network structure was slower despite the similar denaturation temperatures (from DSC). This may have been caused by the larger electrostatic repulsion at neutral pH and resulting in a fine-stranded gel network for the fermentation-derived proteins,

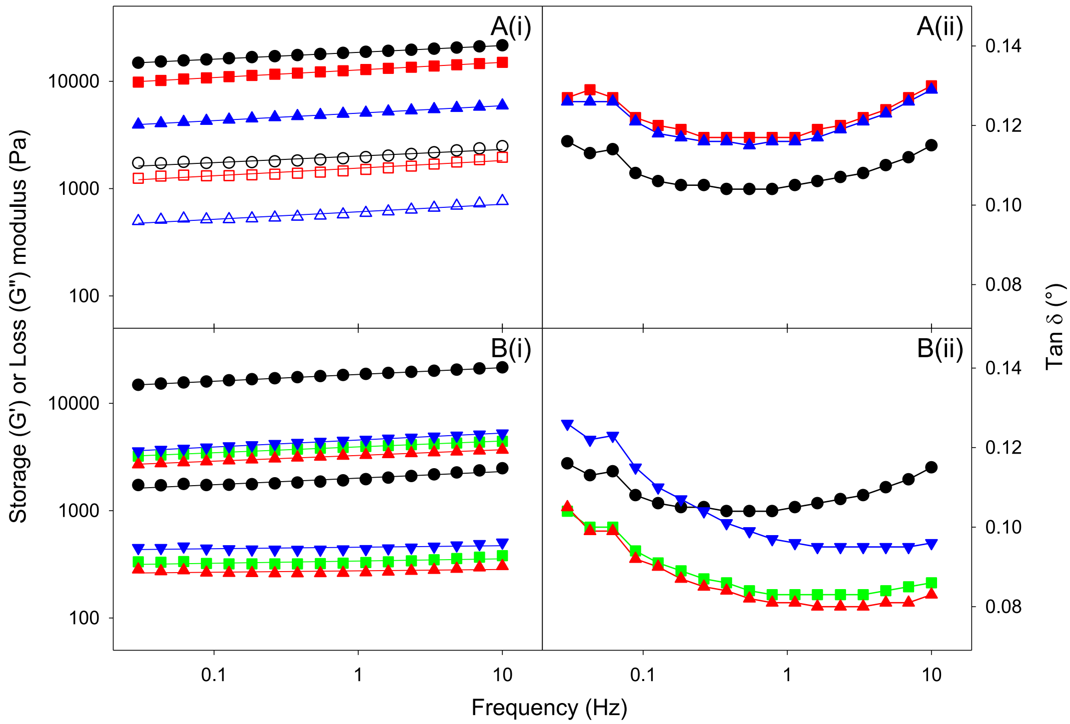

Fig. 3. Frequency sweeps of the set gels. The gels were prepared from β-LG solutions (7.5% w/w in water with 64 mM NaCl) that were held at 20 °C for 5 min, heated from 20 °C to 90 °C at a rate of 5 °C min^{-1}, held at 90 °C for 30 min, cooled from 90 °C to 20 °C at a rate of 5 °C min^{-1}, and finally held at 20 °C for 30 min. A(i) and A(ii): mβ-LG A (●,○), mβ-LG B (■,□) and mβ-LG C (▲,△). B(i) and B(ii): mβ-LG A (●,○), fβ-LG PS (▲,□) fβ-LG FD (▼,△), fβ-LG SD (○,▽). A(i) and B(i) show the storage modulus (G′, solid symbol) and loss modulus (G″, open symbol) against frequency whereas A(ii) and B(ii) show the tan δ against frequency.

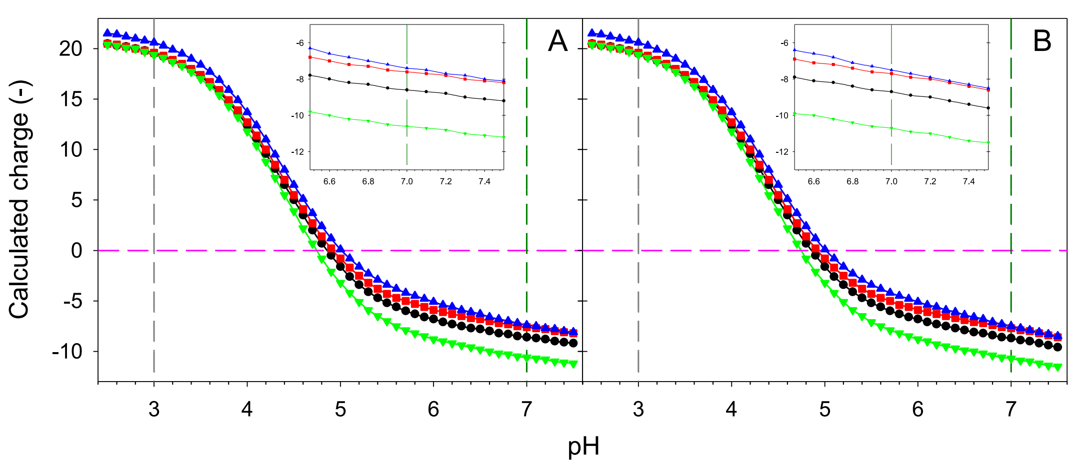

Fig. 4. Calculated net charge with pH for the β-LG samples in reduced form (A) or with two disulphide bonds (B). mβ-LG A (●), mβ-LG B (■) and mβ-LG C (▲), fβ-LG PS/SD/FD (▼). The insert in each figure expands the region around pH 7.0.

accounting for the greater transparency and homogeneous gel structure (Fig. 2) and the greater resemblance to a true gel. The mβ-LG variants may have a mixed fine-stranded and particulate gel structure giving an opaque gel with a distinct particulate structure (Fig. 2), which deviates slightly more from a true gel system and explains the lower elastic contribution upon small oscillatory deformation. An important practical distinction between particulate and fine-stranded whey protein gels is their permeability and water-holding capacity. Particulate gels generally exhibit higher permeability and lower water-holding capacity (Cakır & Foegeding, 2011; Verheul & Roefs, 1998). However, the reduced water-holding ability due to their coarser structure can be partially compensated by increased gel stiffness (Urbonaite et al., 2016).

3.3. Large amplitude oscillatory shear (LAOS) rheological properties of the set gels

Once the gel had been set and held at 20 °C for 30 min, the LAOS rheological properties of the gels were examined. The strain was progressively increased from about 0.1% to 1,000% and G′ was monitored (Fig. 5). For mβ-LG A, mβ-LG B and mβ-LG C, a similar general behaviour was observed where the G′ was unaffected by strain to a certain level, then the G′ progressively decreased with further increases in strain, followed by a sudden abrupt decrease (Fig. 5A(i)). The linear region indicates that the smaller strains are accommodated by the curvature and stretching of the strands during the rotation. Up to this point, the strain will still be within the linear viscoelastic region (LVR) and any changes are reversible. At higher strains, some strands are stretched beyond breaking and exceeding the formation of new junctions resulting in a small decrease in G′, whereas the abrupt decrease indicates that many of the strands are exceeding their stretch limit and rupturing so the gel structure is substantially and irreversibly changed. In the case of a particulate gel network, a reduced number of interactions per mass unit of protein between particulates results in a more gradual gel structure breakdown compared with a homogeneous fine-stranded structure. This transition is supported by the plot of the shear stress versus strain curves that showed a slight curvature just before reaching a maximum stress, and this maximum stress corresponded to the abrupt decrease in G′ and probably corresponds to the yield point of the gel network (Fig. 5B(i)).

Gels from mβ-LG A, mβ-LG B and mβ-LG C started to gradually decline from about the same strain (~2% strain); however, the subsequent abrupt decline where a large number of strands yielded was shorter for mβ-LG A (~40% strain) whereas mβ-LG C was the longest at about 100% strain, with mβ-LG B intermediate at about 90% strain. Interestingly this is the opposite order of the gel stiffness results from SAOS rheology (Fig. 3) where mβ-LG A had the highest G′ and mβ-LG C had the lowest with mβ-LG B intermediate. This suggests that the gel from the mβ-LG A may be the stiffest, but it had a greater number of weaker interactions holding the structure, whereas mβ-LG C was less stiff but more strands were stronger or could be straightened/stretched further so that the gel yielded at a higher strain, while mβ-LG B was intermediate. The curvature before the marked fall in G′ was less for mβ-LG C than mβ-LG A or mβ-LG B suggesting that although the strands could be stretched/straightened further, more of them yielded more abruptly. Interestingly, the stress where the gels yielded was similar for all three mβ-LG variants at about 3,000 Pa.

The strain versus G′ curves for the fβ-LG gels (Fig. 5A(ii)) were different from those of the mβ-LG A variant. Where the LVR for mβ-LG A extended to about 2% strain, with curvature to about 40% and then an abrupt decrease, all three fβ-LG gels had a long LVR extending to about 100% strain, and then an abrupt decrease in G′ as the gel yielded. This is consistent with a fine-stranded network, where the homogeneity in the gel structure is reflected in an abrupt breakdown after exceeding the stretch limit. The fβ-LG PS and fβ-LG FD showed a small but significant increase in G′ just prior to the abrupt decrease. This was also observed for the G″ (results not shown) indicating the samples had a Type IV strong strain overshoot as described by Hyun et al. (2002, 2011). This type of strain overshoot was also observed for some associative polymers, and it was suggested that as the strain is increased, some molecular interactions disengage allowing hydrophobic groups to interact with neighbouring polymer chains, increasing the number of intermolecular interactions and consequently the G′. Further increasing the strain will eventually disrupt the network structure and the G′ will decrease (Tirtaatmadja et al., 1997).

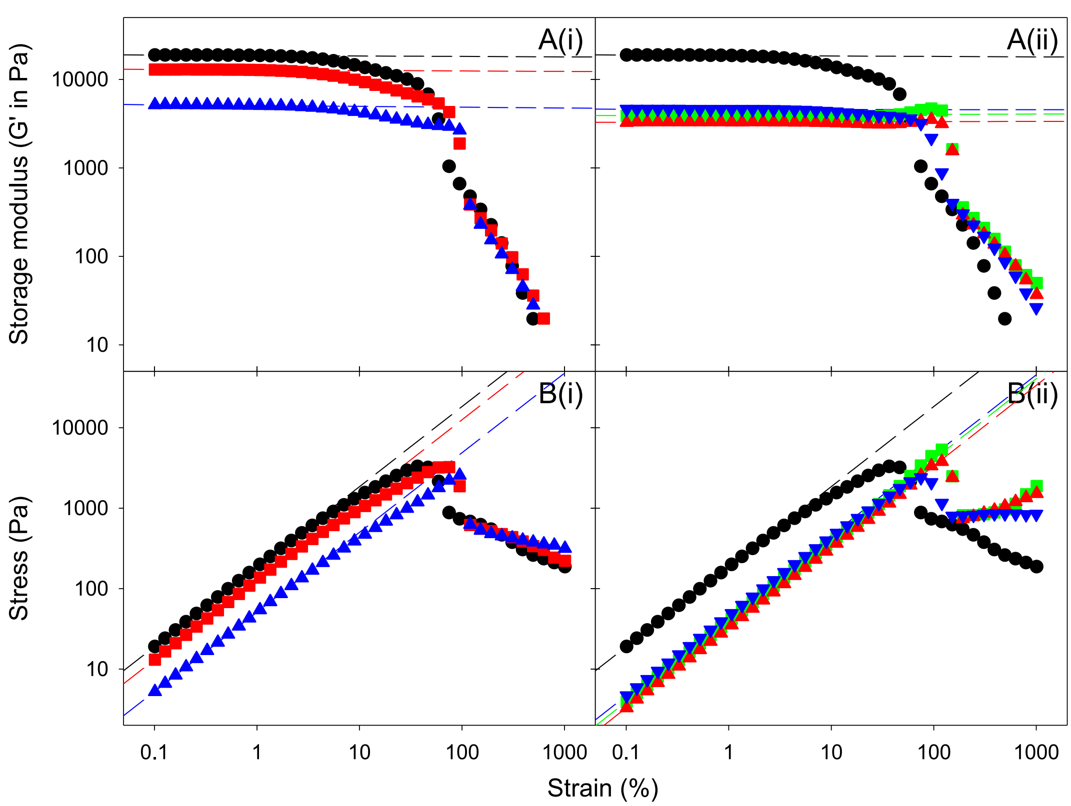

Fig. 5. Strain versus storage modulus (A) and strain versus stress (B) curves. A(i), B(i): mβ-LG A (●), mβ-LG B (■) and mβ-LG C (▲); A(ii), B(ii): mβ-LG A (●), fβ-LG PS (■) fβ-LG FD (▲), fβ-LG SD (▼).

The G′ for the fβ-LG SD slightly decreased just before the abrupt decrease. When looking at the stress versus strain curves, unlike the gels from mβ-LG A, mβ-LG B and mβ-LG C that showed a curvature before the abrupt decrease in stress, the fβ-LG PS, fβ-LG FD and fβ-LG SD showed a very linear stress versus strain relationship up to the point the gels yielded. Compared with the yield stress for mβ-LG A, the yield stress for fβ-LG PS and fβ-LG FD were slightly higher and that of the fβ-LG SD was slightly lower (Fig. 5B(ii)). These results suggest that for mβ-LG A, mβ-LG B and mβ-LG C there was a progressive microstructural breakdown before an abrupt yielding, whereas in the fermentation-derived samples most strands stretched and then yielded simultaneously. As observed in the gelation profiles, the large strain properties of the fβ-LG samples were closer to the mβ-LG C than mβ-LG A variant from which they were derived, but even mβ-LG C variant had some curvature in the G′ versus strain and stress versus strain sweeps.

3.4. Lissajous curves

Lissajous plots allow the evaluation of the microstructure breakdown during LAOS measurements, with the shape of the plots giving additional microstructural information to that obtained from G′ and G″ in a typical oscillatory experiment. From the LAOS results, elastic Lissajous plots were constructed by plotting the stress versus strain, as well as the elastic and viscous contributions (Fig. 6). The area within the Lissajous curve corresponds to the energy dissipated during one complete cycle of the oscillatory strain that is applied. Therefore, a perfect viscous material produces a circle, and a perfect elastic material produces a straight line with a positive slope. Linear viscoelastic materials will be intermediate and produce an ellipse, whereas a perfect plastic material will produce a square-shaped plot. Materials with a complex microstructure and breakdown during oscillatory shear can display a combination of these shapes, and evaluating these shapes can give information on the structure of the material (Ewoldt et al., 2010; Ewoldt et al., 2008; Schreuders et al., 2021; Sridharan et al., 2021).

For the gels from mβ-LG A, mβ-LG B and mβ-LG C, at low strains (1% shown in Fig. 6(i)), the gels displayed very thin perfectly elliptical shapes with a very small area within the curves. The symmetrical nature of the ellipses indicates a linear viscoelastic gel. The narrow nature of the ellipse indicates a very elastic gel structure that was very close to that expected for a perfect elastic material. At slightly higher strain (11% shown in Fig. 6(ii)), the ellipse was still narrow with a very small area, but was slightly tilted at the maximum deformation, producing a slightly inverted sigmoidal curve. This indicates some deviation from linear viscoelastic behaviour and a slight strain-hardening effect during oscillation cycles. Up to this strain, the three mβ-LG variants behaved similarly. At 75% strain, a more pronounced inverted sigmoidal curve was observed. The strain-hardening effect may be a result of particulates starting to collide with each other, and/or, at a smaller scale, an increased resistance of the stranded polymers against deformation. For the B and C variants, the inverted sigmoidal curve still had a small area, whereas the area for the A variant increased. At higher strains, the curves gradually approached those close to perfect plastic, with the C

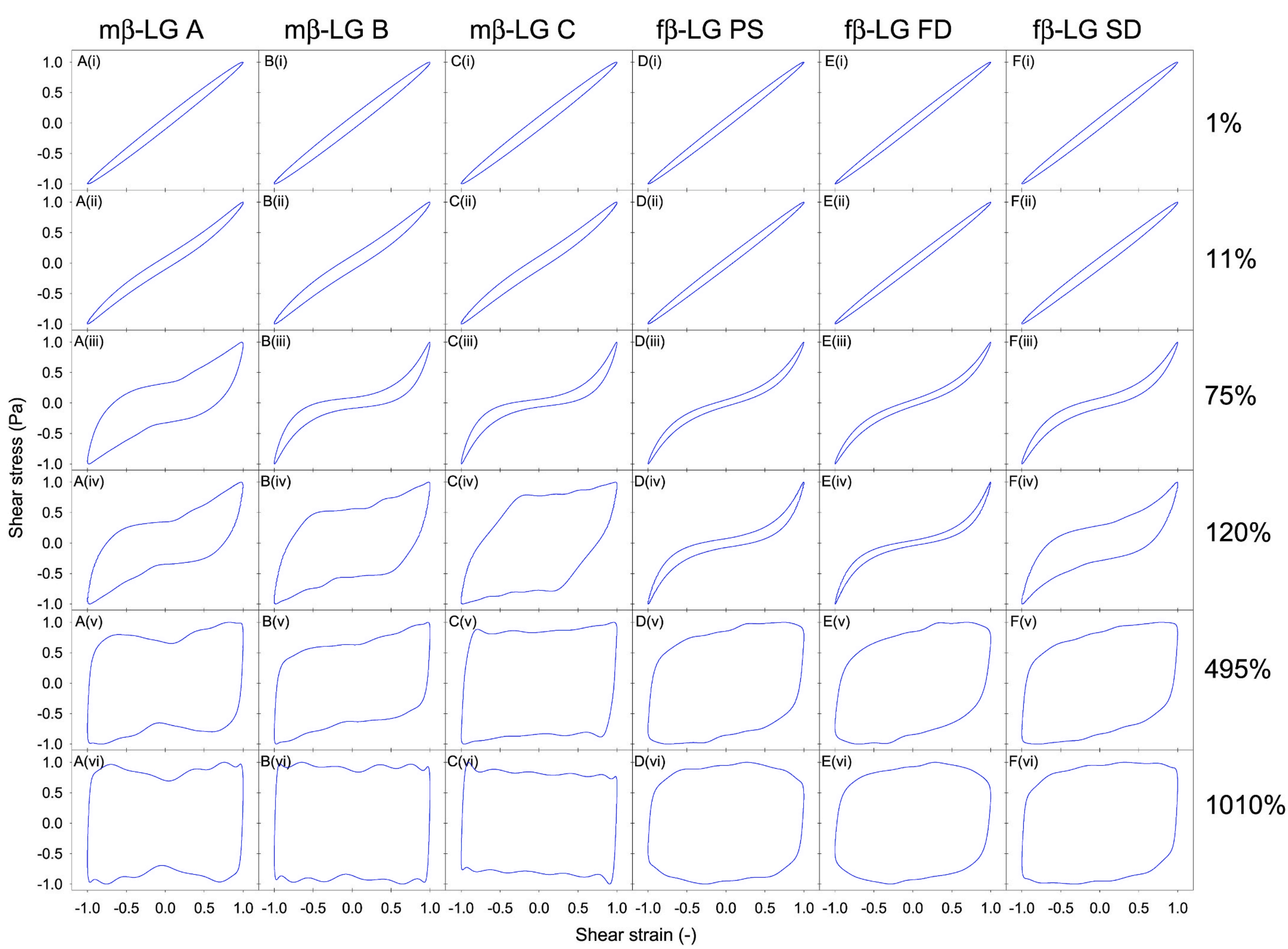

Fig. 6. Elastic Lissajous figures of A: mβ-LG A, B: mβ-LG B, C: mβ-LG C, D: fβ-LG PS, E: fβ-LG FD, and F: fβ-LG SD as a function of strain (i: 1%, ii: 11%, iii: 75%, iv: 120%, v: 495%, and vi: 1010%) at a frequency of 1 Hz and at 20 °C.

variant attaining this state at lower strains than the A variant, with the B variant intermediate.

The Lissajous plots for fβ-LG PS, fβ-LG FD and fβ-LG SD at each strain were very similar, except at a 120% strain amplitude (Fig. 6D–F). The somewhat earlier widening of the curve for the fβ-LG SD sample indicates earlier energy dissipation and a somewhat more brittle gel network. This may be explained by spray-drying induced partial aggregation, which is consistent with a lower denaturation enthalpy (Table 2). When comparing the Lissajous plots of mβ-LG A with those of the fermentation-derived proteins, larger differences were observed. At 1% strain (Fig. 6(i)), all samples displayed very thin perfectly elliptical shapes with a very low area within the curves, indicating linear viscoelastic gels with a very elastic structure close to that of a perfect elastic material. At slightly higher strain (11%, Fig. 6(ii)), some differences between gels from mβ-LG A and the fβ-LG were observed. Where mβ-LG A showed a narrow curve that was slightly tilted at the maximum deformation, producing a slightly inverted sigmoidal curve, the three fermentation-derived variants still displayed perfectly elliptical curves with a very small area almost identical to that observed at 1% strain. This indicates that the fermentation-derived variants maintained a linear viscoelastic gel behaviour whereas the mβ-LG A had some deviation from this behaviour.

At 75% strain (Fig. 6(iii)), mβ-LG A and all fβ-LG samples displayed inverted sigmoidal curves, although the mβ-LG A had an increased area within the curve whereas the fermentation-derived proteins maintained a low area. The increased area of mβ-LG A, indicating a higher degree of energy dissipation, can be explained by the gradual microstructural breakdown of the particulate network. At higher strains, the curve for mβ-LG A gradually approached that of a perfect plastic, whereas those for the fermentation-derived samples produced more elliptical curves suggesting a more viscous or viscoelastic state.

The ratio of the dissipated energy and that expected for a perfect plastic material gives the energy dissipation ratio (φ). This dimensionless φ compares the measured response with that of a perfect plastic, which has the highest possible energy dissipation. Therefore, $\varphi = 0$ represents a perfect elastic material as no energy is dissipated, $\varphi = 1$ represents a perfect plastic material as this has the maximum energy dissipation, and $\varphi = \pi/4$ (~0.79) represents a Newtonian fluid (Ewoldt et al., 2010; Ptaszek, 2014; Schreuders et al., 2021; Schreuders et al., 2022). The φ can be calculated from the loss modulus and the maximum stress at an applied strain amplitude using Equation (4) as has been described previously (Kornet et al., 2022; Schreuders et al., 2022). The energy dissipation ratio against strain for mβ-LG A, mβ-LG B and mβ-LG C are shown in Fig. 7A. The dissipation ratio for mβ-LG A started increasing at a lower strain (about 50%) than for mβ-LG B and mβ-LG C, which both started increasing at a strain of about 100%. At strains above about 100%, the dissipation ratio for mβ-LG A and mβ-LG B were similar at each strain and lower than mβ-LG C, although all three samples converged at the highest strain values (Fig. 7A).

The energy dissipation ratio against strain for mβ-LG A, fβ-LG PS, fβ-LG FD and fβ-LG SD are shown in Fig. 7B. The dissipation ratio for the fβ-LG samples started increasing at a much higher strain (~95% or higher) than for mβ-LG A (about 50%), which indicates that the fβ-LG had a highly elastic response with minimal energy dissipation over a wider strain range. The fβ-LG SD started increasing at a lower strain (~95%) than fβ-LG FD (~150%), and the fβ-LG PS was between these two (~120%). At strains above about 200%, the dissipation ratio for mβ-LG A and all fβ-LG samples were similar to each other. Overall, these results indicate that at medium deformation between 50 and 95%, only the mβ-LG A gel structure started dissipating a significant proportion of its energy, whereas higher deformations were required for the mβ-LG B, mβ-LG C and fβ-LG gels to dissipate a significant proportion of its energy. Based on the earlier strain sweep results (Fig. 5), it is likely that in between 95 and 192%, the bovine mβ-LG B and mβ-LG C start to deviate from the fermentation-derived fβ-LG PS, fβ-LG FD and fβ-LG SD.

4. Conclusions

This study demonstrated that small differences in the amino acid sequence of β-LG significantly impact its heat-set gelling behaviour and gel material properties. Bovine mβ-LG A, mβ-LG B and mβ-LG C variants had different gelation onsets and kinetics, likely due to different thiol reactivity, resulting in differences in gel stiffness and ductility. All gels from mβ-LG variants appeared opaque, indicating a particulate gel network. The fβ-LG A variants, produced via precision fermentation either at laboratory or pilot scale and either spray dried or freeze dried, showed a later gelation onset and a lower gel stiffness compared to the mβ-LG variants. These fβ-LG gels were also more elastic (i.e., smaller tan δ) and ductile, and they appeared translucent, suggesting a fine-stranded network. Given the low level of impurities and the standardized ionic strength, it is unlikely that the difference in gelation and gel properties are explained by compositional differences between the samples. The fine-stranded network is hypothesized to result from higher electrostatic repulsion due to a more negative surface charge, caused by the presence of glutamic acid (E) at the extended N-terminus.

Different gelling behaviour and gel structures can be obtained from

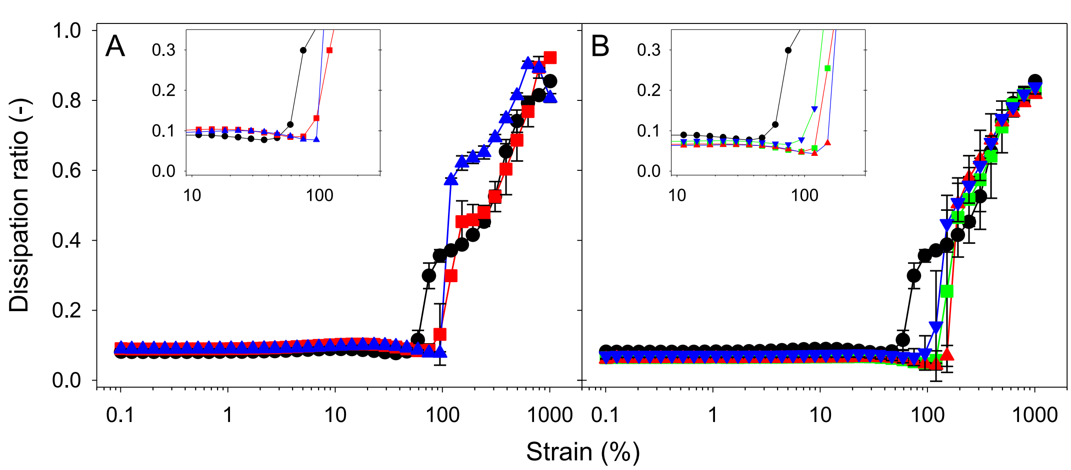

Fig. 7. A: Dissipation ratio against strain for gels formed from mβ-LG A (●), mβ-LG B (■) and mβ-LG C (▲) at a frequency of 1 Hz and at 20 °C. (B) Dissipation ratio against strain for gels formed from mβ-LG A (●), fβ-LG PS (■) fβ-LG FD (▲), fβ-LG SD (▼) at a frequency of 1 Hz and at 20 °C. Inserts show the changes from strains of 10–100. Error bars represent the standard deviations of repeated measurements.

β-LG as a result of minor sequence variations, whether naturally occurring or induced in the fermentation process. By selectively extracting mβ-LG variants or utilizing precision fermentation for further engineering of the fβ-LG molecule, it is possible to tailor the heat-set gelation functionality of these proteins. This allows for the design of proteins capable of forming firm and brittle gels, as well as less firm, more ductile, fine-stranded gels, which may be advantageous for controlling e.g., water-holding capacity of the food matrix. This advanced control over gel properties opens new avenues for food science, enhancing both ingredient performance and versatility.

CRediT authorship contribution statement

Zheng Pan: Writing – original draft, Validation, Methodology, Investigation, Formal analysis, Conceptualization. **Remco Kornet:** Writing – original draft, Validation, Resources, Methodology, Investigation, Formal analysis, Conceptualization. **Sheelagh Hewitt:** Writing – review & editing, Supervision. **Alan Welman:** Writing – review & editing, Supervision. **Jeremy P. Hill:** Writing – review & editing, Supervision, Project administration. **Marcel Wubbolts:** Writing – review & editing, Supervision, Resources, Project administration. **Stephen Mitchell:** Supervision, Project administration. **Warren C. McNabb:** Writing – review & editing, Supervision. **Aiqian Ye:** Writing – review & editing, Supervision. **Alejandra Acevedo-Fani:** Writing – review & editing, Supervision. **Skelte G. Anema:** Writing – review & editing, Writing – original draft, Validation, Supervision, Resources, Methodology, Investigation, Formal analysis, Conceptualization.

Declaration of competing interest

The authors declare the following financial interests/personal relationships which may be considered as potential competing interests: Authors Sheelagh Hewitt, Alan Welman, Jeremy P. Hill, Stephen Mitchell and Skelte G. Anema are employees of the Fonterra Dairy Cooperative, which manufactures dairy ingredients and products. Authors Remco Kornet and Marcel Wubbolts are employees of Vivici BV, which manufactures fermentation-derived proteins.

Acknowledgements

The authors thank Abraham Chawanji for the confocal microscopy images.

Data availability

Data will be made available on request.

References

Anandharamakrishnan, C., Rielly, C. D., & Stapley, A. G. F. (2007). Effects of process variables on the denaturation of whey proteins during spray drying. *Drying Technology, 25*, 799–807.

Anema, S. G., Lee, S. K., & Klostermeyer, H. (2006). Effect of protein, nonprotein-soluble components, and lactose concentrations on the irreversible thermal denaturation of β-lactoglobulin and α-lactalbumin in skim milk. *Journal of Agricultural and Food Chemistry, 54*, 7339–7348.

Augustin, M. A., Hartley, C. J., Maloney, G., & Tyndall, S. (2023). Innovation in precision fermentation for food ingredients. *Critical Reviews in Food Science and Nutrition*, 1–21.

Bendall, J. G., Chawanji, A. S., Fong, B. Y., Andrewes, P., Ma, L., MacGibbon, A. K. H., et al. (2024). "Milk on ice": A detailed analysis of ernest shackleton's century-old whole milk powder in comparison with modern counterparts. *Journal of Dairy Science, 107*, 1311–1333.

Bikker, J. F., Anema, S. G., Li, Y., & Hill, J. P. (2000). Rheological properties of acid gels prepared from heated milk fortified with whey protein mixtures containing the A, B and C variants of β-lactoglobulin. *International Dairy Journal, 10*, 723–732.

Cakır, E., & Foegeding, E. A. (2011). Combining protein micro-phase separation and protein–polysaccharide segregative phase separation to produce gel structures. *Food Hydrocolloids, 25*, 1538–1546.

Chaudhuri, T. K., Horii, K., Yoda, T., Arai, M., Nagata, S., Terada, T. P., et al. (1999). Effect of the extra N-terminal methionine residue on the stability and folding of recombinant α-lactalbumin expressed in Escherichia coli. *Journal of Molecular Biology, 285*, 1179–1194.

Creamer, L. K., & Harris, D. P. (1997). Relationship between milk protein polymorphism and physico-chemical properties. In *International dairy federation special issue 9702. Milk protein polymorphism* (pp. 110–123). Brussels: International Dairy Federation.

Ewoldt, R. H., Clasen, C., Hosoi, A. E., & McKinley, G. H. (2007). Rheological fingerprinting of gastropod pedal mucus and synthetic complex fluids for biomimicking adhesive locomotion. *Soft Matter, 3*, 634–643.

Ewoldt, R. H., Hosoi, A. E., & McKinley, G. H. (2008). New measures for characterizing nonlinear viscoelasticity in large amplitude oscillatory shear. *Journal of Rheology, 52*, 1427–1458.

Ewoldt, R. H., Winter, P., Maxey, J., & McKinley, G. H. (2010). Large amplitude oscillatory shear of pseudoplastic and elastoviscoplastic materials. *Rheologica Acta, 49*, 191–212.

Farrell, H. M., Jimenez-Flores, R., Bleck, G. T., Brown, E. M., Butler, J. E., Creamer, L. K., et al. (2004). Nomenclature of the proteins of cows' milk - sixth revision. *Journal of Dairy Science, 87*, 1641–1674.

Food and Drug Administration. (2015). *Scientific considerations in demonstrating biosimilarity to a reference product: Guidance for industry. U.S. Department of health and human services*. USA: Food and Drug Administration.

Gai, N., Uniacke-Lowe, T., O'Regan, J., Faulkner, H., & Kelly, A. L. (2021). Effect of protein genotypes on physicochemical properties and protein functionality of bovine milk: A review. *Foods, 10*, 2409.

Hairunnisa Ramli, H., Zainal, N. F. A., Hess, M., & Chan, C. H. (2022). Basic principle and good practices of rheology for polymers for teachers and beginners. *Chemistry Teacher International, 4*, 307–326.

Hilgendorf, K., Wang, Y., Miller, M. J., & Jin, Y.-S. (2024). Precision fermentation for improving the quality, flavor, safety, and sustainability of foods. *Current Opinion in Biotechnology, 86*, Article 103084.

Hoppenreijs, L. J. G., Annibal, A., Vreeke, G. J. C., Boom, R. M., & Keppler, J. K. (2024). Food proteins from yeast-based precision fermentation: Simple purification of recombinant β-lactoglobulin using polyphosphate. *Food Research International, 176*, Article 113801.

Huang, X. L., Catignani, G. L., Foegeding, E. A., & Swaisgood, H. E. (1994). Comparison of the gelation properties of β-lactoglobulin genetic variants A and B. *Journal of Agricultural and Food Chemistry, 42*, 1064–1067.

Hyun, K., Kim, S. H., Ahn, K. H., & Lee, S. J. (2002). Large amplitude oscillatory shear as a way to classify the complex fluids. *Journal of Non-newtonian Fluid Mechanics, 107*, 51–65.

Hyun, K., Wilhelm, M., Klein, C. O., Cho, K. S., Nam, J. G., Ahn, K. H., et al. (2011). A review of nonlinear oscillatory shear tests: Analysis and application of large amplitude oscillatory shear (Laos). *Progress in Polymer Science, 36*, 1697–1753.

Keppler, J. K., Heyse, A., Scheidler, E., Uttinger, M. J., Fitzner, L., Jandt, U., et al. (2021). Towards recombinantly produced milk proteins: Physicochemical and emulsifying properties of engineered whey protein beta-lactoglobulin variants. *Food Hydrocolloids, 110*, Article 106132.

Keppler, J. K., Sönnichsen, F. D., Lorenzen, P.-C., & Schwarz, K. (2014). Differences in heat stability and ligand binding among β-lactoglobulin genetic variants A, B and C using ^{1}H NMR and fluorescence quenching. *Biochimica et Biophysica Acta (BBA) - Proteins & Proteomics, 1844*, 1083–1093.

Khalesi, H., Sun, C., He, J., Lu, W., & Fang, Y. (2021). The role of amyloid fibrils in the modification of whey protein isolate gels with the form of stranded and particulate microstructures. *Food Research International, 140*, Article 109856.

Kornet, R., Penris, S., Venema, P., van der Goot, A. J., Meinders, M. B. J., & van der Linden, E. (2021). How pea fractions with different protein composition and purity can substitute WPI in heat-set gels. *Food Hydrocolloids, 120*, Article 106891.

Kornet, R., Sridharan, S., Venema, P., Sagis, L. M. C., Nikiforidis, C. V., van der Goot, A. J., et al. (2022). Fractionation methods affect the gelling properties of pea proteins in emulsion-filled gels. *Food Hydrocolloids, 125*, Article 107427.

Mailliart, P., & Ribadeau-Dumas, B. (1988). Preparation of b-lactoglobulin and b-lactoglobulin-free proteins from whey retentate by NaCl salting out at low pH. *Journal of Food Science, 53*, 743–745.

Manderson, G. A., Creamer, L. K., & Hardman, M. J. (1999). Effect of heat treatment on the circular dichroism spectra of bovine beta-lactoglobulin A, B, and C. *Journal of Agricultural and Food Chemistry, 47*, 4557–4567.

Manderson, G. A., Hardman, M. J., & Creamer, L. K. (1998). Effect of heat treatment on the conformation and aggregation of β-lactoglobulin A, B, and C. *Journal of Agricultural and Food Chemistry, 46*, 5052–5061.

Manderson, G. A., Hardman, M. J., & Creamer, L. K. (1999). Effect of heat treatment on bovine beta-lactoglobulin A, B, and C explored using thiol availability and fluorescence. *Journal of Agricultural and Food Chemistry, 47*, 3617–3627.

Minj, S., & Anand, S. (2020). Whey proteins and its derivatives: Bioactivity, functionality, and current applications. *Dairy, 1*, 233–258.

Nielsen, M. B., Meyer, A. S., & Arnau, J. (2023). The next food revolution is here: Recombinant microbial production of milk and egg proteins by precision fermentation. *Annual Review of Food Science and Technology*.

Panick, G., Malessa, R., & Winter, R. (1999). Differences between the pressure- and temperature-induced denaturation and aggregation of β-lactoglobulin A, B, and AB monitored by FT-IR spectroscopy and small-angle X-ray scattering. *Biochemistry, 38*, 6512–6519.

Paulsson, M., & Dejmek, P. (1990). Thermal-denaturation of whey proteins in mixtures with caseins studied by differential scanning calorimetry. *Journal of Dairy Science, 73*, 590–600.

Paulsson, M., Hegg, P. O., & Castberg, H. B. (1985). Thermal stability of whey proteins studied by differential scanning calorimetry. *Thermochimica Acta, 95*, 435–440.

Picout, D. R., & Ross-Murphy, S. B. (2003). Rheology of biopolymer solutions and gels. *The Scientific World Journal, 3*, 105–121.
Protein Calculator v3.4. (2013). Accessed: 1 June 2024. https://protcalc.sourceforge.net/.
Ptaszek, P. (2014). Large amplitudes oscillatory shear (Laos) behavior of egg white foams with apple pectins and xanthan gum. *Food Research International, 62*, 299–307.
Qin, B. Y., Bewley, M. C., Creamer, L. K., Baker, E. N., & Jameson, G. B. (1999). Functional implications of structural differences between variants A and B of bovine β-lactoglobulin. *Protein Science, 8*, 75–83.
Ruegg, M., Moor, U., & Blanc, B. (1977). A calorimetric study of thermal denaturation of whey proteins in simulated milk ultrafiltrate. *Journal of Dairy Research, 44*, 509–520.
Saadi, S., Makhlouf, C., Nacer, N. E., Halima, B., Faiza, A., Kahina, H., et al. (2024). Whey proteins as multifunctional food materials: Recent advancements in hydrolysis, separation, and peptidomimetic approaches. *Comprehensive Reviews in Food Science and Food Safety, 23*, Article e13288.
Saikhwan, P., Mercadé-Prieto, R., Chew, Y. M. J., Gunasekaran, S., Paterson, W. R., & Wilson, D. I. (2010). Swelling and dissolution in cleaning of whey protein gels. *Food and Bioproducts Processing, 88*, 375–383.
Sawyer, W. H. (1968). Heat denaturation of bovine β-lactoglobulins and relevance of disulfide aggregation. *Journal of Dairy Science, 51*, 323–329.
Schreuders, F. K. G., Sagis, L. M. C., Bodnár, I., Boom, R. M., & van der Goot, A. J. (2022). Non-linear rheology reveals the importance of elasticity in meat and meat analogues. *Scientific Reports, 12*, 1334.
Schreuders, F. K. G., Sagis, L. M. C., Bodnár, I., Erni, P., Boom, R. M., & van der Goot, A. J. (2021). Small and large oscillatory shear properties of concentrated proteins. *Food Hydrocolloids, 110*, Article 106172.
Schultz, D. A., & Baldwin, R. L. (1992). Cis proline mutants of ribonuclease A. I. thermal stability. *Protein Science, 1*, 910–916.
Sridharan, S., Meinders, M. B. J., Sagis, L. M., Bitter, J. H., & Nikiforidis, C. V. (2021). Jammed emulsions with adhesive pea protein particles for elastoplastic edible 3D printed materials. *Advanced Functional Materials, 31*, Article 2101749.
Stading, M., & Hermansson, A.-M. (1990). Viscoelastic behaviour of β-lactoglobulin gel structures. *Food Hydrocolloids, 4*, 121–135.
Swaisgood, H. E. (1982). Chemistry of milk protein. In P. F. Fox (Ed.), *Developments in dairy chemistry-1* (pp. 1–59). London: Elsevier Applied Science.
Swaisgood, H. E. (2003). Chemistry of the caseins. In P. F. Fox, & P. L. H. McSweeney (Eds.), *Advanced dairy chemistry - 1 proteins: Part A* (pp. 139–201). Boston, MA: Springer US.
Thresher, W. C., & Harris, D. P. (1997). Interactions of β-lactoglobulin variants with κ-casein and DTNB: Formation of a covalent comple. In *International dairy federation special issue 9702. Milk protein polymorphism* (pp. 138–145). Brussels: International Dairy Federation.
Tirtaatmadja, V., Tam, K. C., & Jenkins, R. D. (1997). Superposition of oscillations on steady shear flow as a technique for investigating the structure of associative polymers. *Macromolecules, 30*, 1426–1433.
Turck, D., Bohn, T., Castenmiller, J., de Henauw, S., Hirsch-Ernst, K. I., Maciuk, A., et al. (2024). Guidance on the scientific requirements for an application for authorisation of a novel food in the context of Regulation (EU) 2015/2283. *EFSA Journal, 22*, Article e8961.
Urbonaite, V., van der Kaaij, S., de Jongh, H. H. J., Scholten, E., Ako, K., van der Linden, E., et al. (2016). Relation between gel stiffness and water holding for coarse and fine-stranded protein gels. *Food Hydrocolloids, 56*, 334–343.
Verheul, M., & Roefs, S. P. F. M. (1998). Structure of whey protein gels, studied by permeability, scanning electron microscopy and rheology. *Food Hydrocolloids, 12*, 17–24.